JSME Journal Template

Reducer-integrated motor using simultaneous engagement of gear pairs with small and no differences in teeth number

Tatsuro TERAKAWA*, Masaharu KOMORI*, Shouta TAMURA**,
Ryo KATAOKA** and Yuya MORITA*
* Department of Mechanical Engineering and Science, Kyoto University
Kyoto daigaku-katsura, Nishikyo-ku, Kyoto 615-8540, Japan
E-mail: terakawa.tatsuro.63c@kyoto-u.jp
**Undergraduate School of Engineering Science, Kyoto University
Yoshida Honmachi, Sakyo-ku, Kyoto 606-8501, Japan

Received 16 August 2013

Abstract
The motors for industrial robots and transporting robots require high-precision positioning, large torque output, and downsizing. However, conventional motors have difficulties in downsizing or supporting large torque. In this research, we propose a novel reducer-integrated motor to solve the problems of existing motors. The proposed reducer-integrated motor has a differential gear mechanism using the simultaneous engagement of two kinds of external and internal gear pairs: one with a small difference in teeth number and the other with no difference in teeth number. Inside the reducer, linear actuators are installed. Two gear pairs with no difference in teeth number are fixed on the base and the gear pair with a small difference in teeth number is set between them. When the linear actuators revolve the external gear, the two kinds of the gear pairs engage simultaneously and the internal gear of the gear pair with a small difference in teeth number outputs the rotation. It is thought that the structure of the proposed motor can realize downsizing of the entire motor system, high load-supporting capacity, and high stiffness. In this paper, the structure and movement of the proposed motor are explained. The geometrical conditions for simultaneous engagement of the two gear pairs with small and no differences in teeth number are clarified. Through the discussion on the solution satisfying the conditions and the relation with the bending strength, a design method for the reducer of this motor is proposed. An experiment conducted on a prototype verifies that the proposed motor works as expected.

Key words : Motor, Reducer, Differential gear mechanism, Design method, Internal gear

1. Introduction

To improve the performance of industrial robots and transporting robots, motors with high-precision positioning and large torque output are required. To meet these requirements, electromagnetic motors are often used with reducers, because the motors themselves have high-speed and low-torque output. However, the conventional reducers that utilize spur gear pairs or planetary gear mechanisms tend to be large and heavy, because they need multistage gear trains to gain high reduction ratios. This means that the entire motor system becomes large and heavy.

On the other hand, reducers with high reduction ratios in a single stage can be manufactured with smaller volume and weight. One example is the reducer using an inscribed planetary gear, or a KHV planetary gear (Kinki Gear Association ed., 1971; Yu, 1987, 1988; Morozumi, 1989). This reducer consists of an external and internal gear pair with one or a few differences in teeth number and a crankshaft revolving the external gear (Fig. 1). When the motor rotates the crankshaft, the external gear revolves around the internal circumference of the internal gear with tooth engagement. The external gear rotates relative to the internal gear by the difference in teeth number per one revolution. By using this relative rotation as output, the reducer realizes a high reduction ratio in a single stage. Therefore, the reducer using the inscribed planetary gear requires fewer gears than do conventional reducers, and consequently achieves downsizing.

Paper No.xx-xxxx
[DOI: 10.1299/xxx.2014xxx000x]

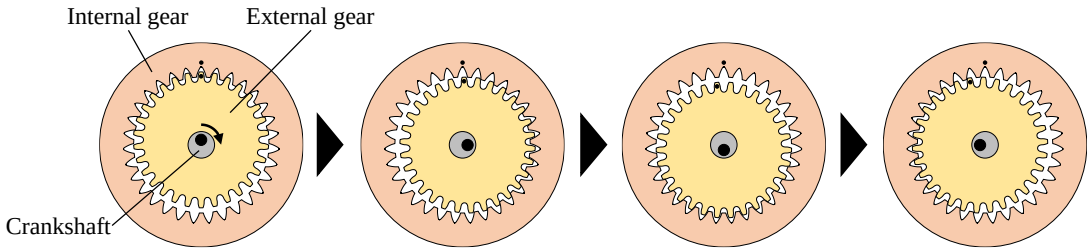

Fig. 1 Movement principle of an inscribed planetary gear

To miniaturize the entire motor system, reducer-integrated motors have been proposed by using reducers of small sizes and high reduction ratios (Ishida et al., 1990; Hayashi et al., 1992; Suzumori and Hori, 1999; Barth, 2000). Motors especially such as cycloid motors (Hayashi et al., 1992) and wobble motors (Suzumori and Hori, 1999) utilize the same principle of an inscribed planetary gear. In these reducer-integrated motors, the internal gear revolves instead of the external gear. These motors have linear actuators to revolve the internal gear by pushing it from the outside to the center. When the internal gear revolves around the external gear, the external gear rotates by the difference in teeth number from the internal gear. Thus, the proposed reducer-integrated motors can output reduced rotation directly from the input of the linear actuators. The advantage is the downsizing of motors over conventional motors, which have separate electromagnetic motors and reducers. However, in the structure of this type of motors, the load torque applied to the output part, i.e., the external gear, brings circumferential force to the linear actuators through the internal gear. Although the linear actuators are suitable to output force in the radial direction, it is difficult for them to support a large force in the circumferential direction. It is also difficult to increase the stiffness in the circumferential direction, and so high-precision positioning becomes a challenge when large torque is required.

To solve this problem, some of the authors previously proposed a reducer-integrated motor using the principle of the strain wave gearing system (Terakawa et al., 2017). That proposed motor is thought to have high load-supporting capacity and high stiffness because the load torque applied to the output part is supported by two internal gears fixed on the base. However, the strain wave gearing system used in the motor requires a special gear, which is an elastic and flexible ringed metal external gear that is not easy to produce. In this research, we propose a novel reducer-integrated motor using only rigid gears to make it easier to produce. This motor utilizes the differential gear mechanism in which the gear pair with a small difference in teeth number and the gear pairs with no difference in teeth number engage simultaneously. This gear mechanism realizes a high reduction ratio and the motor achieves downsizing similarly to the existing reducer-integrated motors. At the same time, the internal gears fixed on the base support the load torque, and then the motor can gain high load-supporting capacity and high stiffness. In this paper, the structure and movement of the proposed motor are explained first. Next, the geometrical conditions for the simultaneous engagement of two gear pairs with small and no differences in teeth number are clarified. Through the discussion on the solutions satisfying the geometrical conditions and the relation with the bending strength, a design method for the reducer of this motor is proposed. The experiment is conducted by using the prototype and verifies that the proposed motor works as expected.

2. Proposal of a reducer-integrated motor

2.1 Structure of the proposed motor

Figure 2 shows the schematic structure of the proposed reducer-integrated motor. As shown in Fig. 2(a), one ringed rigid external gear engages simultaneously with two kinds of internal gears, one A gear and two B gears. The internal A gear has one or a few more teeth than the external gear, and the two internal B gears have the same teeth number as the external gear. The two internal B gears are placed coaxially on both sides of the internal A gear. Figure 2(b) shows sectional views of the entire proposed reducer-integrated motor. Inside the external gear, linear actuators are arranged radially at equal intervals and fixed on the base. Each linear actuator (e.g., linear solenoids driven by an electromagnetic force) can actively elongate and shrink in the radial direction. The external gear can rotate and move in the radial direction freely. The internal A gear is supported to rotate around the central axis. The two internal B gears are fixed on the base and do not rotate.

[DOI: 10.1299/xxx.2014xxx000x]

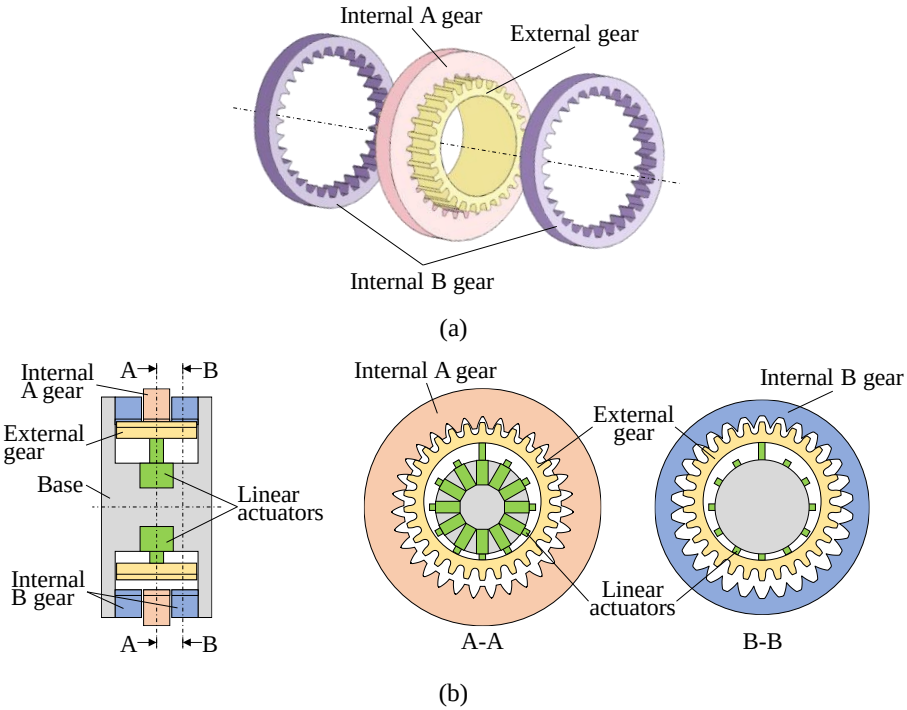

Fig. 2 Structure of the proposed reducer-integrated motor. (a) One external gear, one internal A gear, and two internal B gears. (b) Sectional views of the motor.

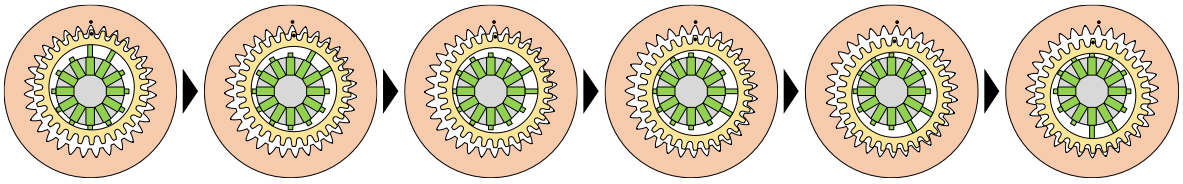

Fig. 3 Rotation of the internal A gear by the revolution of the external gear

2.2 Movement of the proposed motor

Next, we explain the movement of the proposed reducer-integrated motor. When the linear actuators are operated and push the external gear, the external gear moves in the radial direction and engages with the internal A and B gears. Here, we consider the situation where the neighboring two linear actuators are operated at the same time and switched clockwise, as shown in Fig. 3. The teeth number of the external gear is the same as those of the internal B gears fixed on the base, so that the external gear does not rotate but revolves around the internal circumferences of the internal gears. When the external gear revolves, the relative rotation to the internal A gear occurs according to the same principle of the inscribed planetary gear. Because the external gear does not rotate, only internal A gear rotates. Every clockwise revolution of the external gear, that is, every cycle of switching the operating linear actuators, causes rotation of internal A gear by the difference in teeth number from the external gear. The revolution of the external gear by switching linear actuators is set as the input and the rotation of the internal A gear is set as the output, and the reduction ratio R is represented by Eq. (1).

$$R = \frac{z_{2A}}{z_{2A} - z_1} \tag{1}$$

Here, z_1 is the teeth number of the external gear and the internal B gears, and z_{2A} is the teeth number of the internal A gear. The difference in teeth number $z_{2A} - z_1$ is a constant having a small value (e.g., 1 or 2). For the constant $z_{2A} - z_1$, R becomes large in proportion to z_{2A}. This means that the proposed motor can directly output a sufficiently reduced rotation.

[DOI: 10.1299/xxx.2014xxx000x]

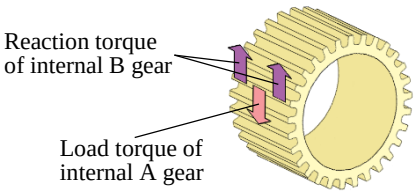

Fig. 4 Torque applied to the external gear by internal A and B gears

When we set the number of linear actuators as n and the switching interval of the operating linear actuators as T, the average rotational speed of the internal A gear is $\bar{N}$, which is calculated as follows:

$$\bar{N} = \frac{1}{nRT} \tag{2}$$

2.3 Characteristics of the proposed motor

In the proposed reducer-integrated motor, the linear actuators are installed inside the reducer. This structure enables the entire motor to be miniaturized. In the conventional reducer-integrated motor, the linear actuators receive the circumferential force from the load torque applied to the output part. On the other hand, in the proposed motor, the load torque applied to the internal A gear is supported by the internal B gears fixed on the base through the external gear, so that the linear actuators do not receive the circumferential force directly. Therefore, the proposed motor can support high load torque and gain high stiffness. Additionally, because the internal B gears are put on both sides of the internal A gear, the load torque on the external gear from the internal A gear and the reaction torque on the external gear from the internal B gears become symmetrical in the axial direction, as shown in Fig. 4. These symmetrical torques are expected to suppress the tilt and torsion of the external gear and increase the stiffness of the motor. It is thought that the proposed reducer-integrated motor can realize downsizing, high load-supporting capacity, and high stiffness, and thus solve the problems of the conventional motors.

Furthermore, the proposed reducer-integrated motor consists of rigid external and internal gears, as seen in common geared reducers. The motor does not need special gears, such as elastic gears or complicated transmission mechanisms, and so it is relatively easy to produce the reducer of the motor. This characteristic contributes to increased practicality and reliability.

3. Conditions for engagement of the gear pairs

The proposed reducer-integrated motor utilizes two kinds of external and internal gear pairs: one with a small difference in teeth number and the other with no difference in teeth number. Here, we should consider how the reducer of the motor is designed. Each gear pair has to satisfy a variety of geometrical conditions for tooth engagement. The proposed motor needs to meet the conditions that the gear pairs with a small difference in teeth number and those with no difference in teeth number share the external gear and its revolution. Thus, the gear pairs of the reducer must satisfy many conditions. Because it is not easy to design the gears, a design method is required. In this section, we clarify the geometrical conditions required for the gear pairs with small and no differences in teeth number to share the external gear. Based on the clarified conditions, we construct a design method for the reducer in the next section.

3.1 Engagement equations for two kinds of external and internal gear pairs

We show the engagement equations for the external gear and the internal A and B gears. Here, the teeth of the external gear and internal A and B gears are assumed to have an involute profile. According to the theory on the engagement of the involute internal and external gears with a difference in teeth number (Yaejima and Yano, 1991), the engagement equation for the external gear and the internal A gear is represented as follows:

$$a_A = m_n \frac{z_{2A} - z_1}{2} \cdot \frac{\cos\alpha}{\cos\alpha_w} \tag{3}$$

[DOI: 10.1299/xxx.2014xxx000x]

$$\mathrm{inv}\,\alpha_w = \mathrm{inv}\,\alpha + 2\tan\alpha \cdot \frac{x_{2A}-x_1}{z_{2A}-z_1} \tag{4}$$

where a_A denotes the center distance between the external gear and the internal A gear, m_n denotes the module of the gears, α denotes the reference pressure angle, α_w denotes the working pressure angle, and x_1, x_{2A} denote the vertical profile shift coefficient of the external gear and the internal A gear, respectively. In this paper, we assume the lateral profile shift coefficient and the backlash to be zero for simplicity. The profile shift coefficient in the following discussions is the vertical coefficient. The function inv is the involute function defined by the following equation.

$$\mathrm{inv}\,\theta = \tan\theta - \theta \tag{5}$$

Next, the engagement equation for the external gear and the internal B gears is discussed. The theory on the engagement of the involute external and internal gear having no difference in teeth number (Morozumi and Yaejima, 1969) gives the equation as follows:

$$a_B = m_n(x_{2B} - x_1)\sin\alpha \tag{6}$$

where a_B denotes the center distance between the external gear and the internal B gears, and x_{2B} denotes the profile shift coefficient of the internal B gears. The variables on the external gear are the same as those in the equations for the external gear and the internal A gear, because the external gear is shared.

In the proposed reducer-integrated motor, the external gear has to engage simultaneously with the internal A and B gears. When internal A and B gears are arranged coaxially, the engagement condition is given by

$$a_A = a_B \tag{7}.$$

In the following discussion, we set $a_A = a_B = a$.

3.2 Conditions for tooth engagement of each gear pair

Next, we discuss the conditions for the engagement in each gear pair of the external gear and the internal A and B gears. As the variables concerning the external gear, internal A gear and B gears, the reference circle diameters d_1, d_{2A}, d_{2B}, the tip circle diameters d_{a1}, d_{a2A}, d_{a2B}, the base circle diameters $d_{b1}, d_{b2A}, d_{\mathrm{b}2B}$, and the tip pressure angles $\alpha_{a1}, \alpha_{a2A}, \alpha_{a2B}$ are given as follows, respectively:

$$d_1 = d_{2\mathrm{B}} = z_1 m_n \tag{8}$$

$$d_{2\mathrm{A}} = z_{2\mathrm{A}} m_n \tag{9}$$

$$d_{a1} = m_n\{z_1 + 2(h_{kg1} + x_1)\} \tag{10}$$

$$d_{a2A} = m_n\{z_{2A} - 2(h_{kg2A} - x_{2A})\} \tag{11}$$

$$d_{a2B} = m_n\{z_1 - 2(h_{kg2B} - x_{2B})\} \tag{12}$$

$$d_{b1} = d_{b2B} = m_n z_1 \cos\alpha \tag{13}$$

$$d_{b2A} = m_n z_{2A} \cos\alpha \tag{14}$$

$$\alpha_{a1} = \cos^{-1}\left(\frac{d_{b1}}{d_{a1}}\right) \tag{15}$$

$$\alpha_{a2A} = \cos^{-1}\left(\frac{d_{b2A}}{d_{a2A}}\right) \tag{16}$$

$$\alpha_{a2B} = \cos^{-1}\left(\frac{d_{b2B}}{d_{a2B}}\right) \tag{17}.$$

Here, $h_{kg1}, h_{kg2A}, h_{kg2B}$ are the addendum coefficients, which are the values of the addendum divided by the module m_n.

[DOI: 10.1299/xxx.2014xxx000x]

3.2.1 Comparison between the tip circle diameter and the base circle diameter in the internal gears

From Eqs. (11)–(14), the following conditions are required for $d_{a2A} > d_{b2A}$ and $d_{a2B} > d_{b2B}$.

$$z_{2A} > \frac{2\left(h_{kg2A} - x_{2A}\right)}{1-\cos\alpha} \tag{18}$$

$$z_1 > \frac{2\left(h_{kg2B} - x_{2B}\right)}{1-\cos\alpha} \tag{19}$$

3.2.2 Positional condition of the tooth tips in the gear pair with a difference in teeth number

In the engagement of the external gear and the internal A gear, in one area the teeth are in engagement (e.g., the upper region in Fig. 2(b)) and in another area the teeth are separate from each other (e.g., the lower region in Fig. 2(b)). Therefore, the tooth tips of the external gear in the engagement area have to be outside the tooth tip of the internal A gear, and the tooth tip of the external gear in the separate area has to be inside the tooth tip of the internal A gear. These conditions are represented by the following equation.

$$d_{a1} + 2a > d_{a2A} > d_{a1} - 2a \Leftrightarrow \frac{2a}{m_n} > z_{2A} - z_1 - 2\left(h_{kg2A} + h_{kg1} - x_{2A} + x_1\right) > -\frac{2a}{m_n} \tag{20}$$

3.2.3 Avoidance of sharp tooth tips

The width of the top land of the external gear and the internal A and B gears has to be positive. The condition is given as follows (Semba, 1972):

$$d_{a1}\left\{\frac{\pi}{2z_1} + \frac{2x_1\tan\alpha}{z_1} + (\mathrm{inv}\,\alpha - \mathrm{inv}\,\alpha_{a1})\right\} > 0 \tag{21}$$

$$d_{a2A}\left\{\frac{\pi}{2z_{2A}} - \frac{2x_{2A}\tan\alpha}{z_{2A}} - (\mathrm{inv}\,\alpha - \mathrm{inv}\,\alpha_{a2A})\right\} > 0 \tag{22}$$

$$d_{a2B}\left\{\frac{\pi}{2z_1} - \frac{2x_{2B}\tan\alpha}{z_1} - (\mathrm{inv}\,\alpha - \mathrm{inv}\,\alpha_{a2B})\right\} > 0 \tag{23}.$$

3.2.4 Contact ratio higher than 1

To transmit the rotation of gears appropriately, the contact ratio has to be higher than 1. When the contact ratio between the external gear and the internal A gear is ε_A and that between the external gear and the internal B gears is ε_B, they are calculated by the following equations (Morozumi, 1989).

$$\varepsilon_A = \frac{\sqrt{{d_{a1}}^2 - {d_{b1}}^2} - \sqrt{{d_{a2A}}^2 - {d_{b2A}}^2} + 2a\sin\alpha_w}{2\pi m_n\cos\alpha} > 1 \tag{24}$$

$$\varepsilon_B = \frac{1}{2\pi}\left\{z_1(\tan\alpha_{a1} - \tan\alpha_{a2B}) + \frac{2a}{m_n\cos\alpha}\right\} > 1 \tag{25}$$

In general, it is preferable for the contact ratios to be larger with respect to the strength and the noise.

3.2.5 Avoidance of involute interference

The engagement of the external and internal gears might cause involute interference, in which the tooth root of the external gear interferes with the tooth tip of the internal gear and the rotation of the gears is interrupted. The condition that involute interference does not occur between the external gear and the internal A and B gears is represented by Eqs. (26) and (27), respectively (Doi et al., 1976; Morozumi and Yaejima, 1969).

$$\frac{z_1}{z_{2A}} > 1 - \frac{\tan\alpha_{a2A}}{\tan\alpha_w} \tag{26}$$

[DOI: 10.1299/xxx.2014xxx000x]

$$\frac{z_1}{2}\cdot\frac{\tan\alpha_{a2B}}{\tan\alpha} > x_{2B} - x_1 \tag{27}$$

3.2.6 Avoidance of trochoid interference

The engagement of the external and internal gear might cause trochoid interference, in which the tooth tip of the external gear interferes with that of the internal gear when moving out of the tooth space and the rotation of the gears is interrupted. The condition that trochoid interference does not occur between the external gear and the internal A gear is as follows (Morozumi, 1989):

$$\frac{z_1}{z_{2A}}\left\{\cos^{-1}\left(\frac{{d_{a2A}}^2-{d_{a1}}^2-4a^2}{4ad_{a1}}\right)+\mathrm{inv}\,\alpha_{a1}-\mathrm{inv}\,\alpha_w\right\}-(\mathrm{inv}\,\alpha_{a2A}-\mathrm{inv}\,\alpha_w)>\cos^{-1}\left(\frac{{d_{a2A}}^2-{d_{a1}}^2+4a^2}{4ad_{a2A}}\right) \tag{28}.$$

For the external gear and the internal B gears with no difference in teeth number, trochoid interference never occurs (Ogino, 1957).

3.2.7 Existence of clearance

When the external and internal gears are in engagement at the deepest part, clearance must exist between the tooth bottom of the external gear and the tooth tip of the internal gear, and between the tooth tip of the external gear and the tooth bottom of the internal gear. When the root circle diameters of the external gear and the internal A and B gears are given as d_{f1}, d_{f2A}, d_{f2B}, respectively, the conditions for clearance are as follows:

$$\begin{cases}\frac{d_{a2A}-d_{f1}}{2}-a>0\\ \frac{d_{a2B}-d_{f1}}{2}-a>0\end{cases}\Leftrightarrow d_{f1}<\min(d_{a2A},d_{a2B})-2a \tag{29}$$

$$\frac{d_{f2A}-d_{a1}}{2}-a>0\Leftrightarrow d_{f2A}>d_{a1}+2a \tag{30}$$

$$\frac{d_{f2B}-d_{a1}}{2}-a>0\Leftrightarrow d_{f2B}>d_{a1}+2a \tag{31}.$$

4. Design method for the reducer

In this section, as mentioned in the introduction of Section 3, we construct a design method for the reducer to satisfy a variety of geometrical conditions clarified in the previous section. First, the basic policy of the design is decided based on the movement principle of the proposed motor by discussing which variables should be mainly treated in the design. Then, by using the characteristics of the set of design solutions satisfying the conditions, a method to acquire the available design solutions from graphs is proposed. Next, the strength of the gears corresponding to those design solutions is examined, and the design solutions realizing excellent strength are shown. Finally, the design algorithm for the reducer is constructed according to these discussions.

4.1 Design policy

One of the indicators of the optimal design for the proposed reducer-integrated motor is to make the center distance between the external and internal gears as small as possible. When linear solenoids, which have a quick response and large force output, are used as the linear actuators of the proposed motor, the output force exponentially decreases with the strokes. Thus, it is preferable to minimize the strokes for efficient operation. The required strokes depend on the eccentricity between the external and internal gear, so that the strokes become small when the center distance is small. Not only with linear solenoids but also with other kinds of linear actuators, it thought to be better to keep the center distance small.

Let us discuss the parameters determining the center distance a. From the engagement equations (3), (4), and (6), a is determined by the parameters of the reference pressure angle α, the difference in teeth number $z_{2A}-z_1$, the module m_n, and the differences in profile shift coefficients $x_{2A}-x_1$ and $x_{2B}-x_1$. The smaller that each parameter becomes, the smaller that a becomes. Reference pressure angle α has a certain degree of design freedom, but the

[DOI: 10.1299/xxx.2014xxx000x]

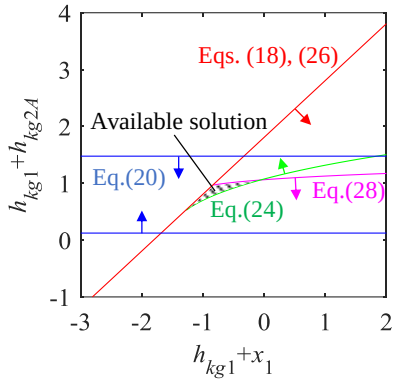

Fig. 5 Region for $h_{kg1}+x_1$ and $h_{kg1}+h_{kg2A}$ satisfying the conditions under a certain value of $x_{2A}-x_1$. The arrows indicate the direction in which each inequality is satisfied.

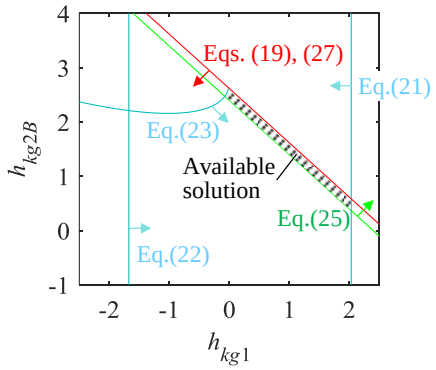

Fig. 6 Region for h_{kg1} and h_{kg2B} satisfying the conditions under a certain value of $x_{2A}-x_1, h_{kg1}+x_1, h_{kg1}+h_{kg2A}$. The arrows indicate the direction in which each inequality is satisfied.

value chosen in standard usage is limited and an extremely small value cannot be used. With respect to $z_{2A}-z_1$, the value is considered to be a small constant in this research. If $z_{2A}-z_1=1$ is chosen, for example, the value achieves the minimum. The value of m_n affects the size of the gears, so that the possible alternatives are limited. As discussed above, making $\alpha, z_{2A}-z_1, m_n$ small is limited. On the other hand, $x_{2A}-x_1$ and $x_{2B}-x_1$ can be small as far as the engagement of each gear pair is established. It is favorable to set these parameters at the center of the discussion in the design. Therefore, we mainly aim to make a small by keeping the differences in the profile shift coefficient as small as possible. Note that $x_{2A}-x_1$ and $x_{2B}-x_1$ are not independent of each other, but one is determined dependently on the other from Eq. (7).

Based on the discussion above, we consider the situation where the values of α, m_n, z_1, z_{2A} are given and $x_{2A}-x_1$ is assumed to be a certain value k. In this situation, Eqs. (18), (20), (24), (26), and (28) become inequalities using $h_{kg1}+x_1$ and $h_{kg1}+h_{kg2A}$ as variables. We propose a graph where the horizontal axis is $h_{kg1}+x_1$ and the vertical axis is $h_{kg1}+h_{kg2A}$ in order to make the solution region for the conditions easy to understand. As an example, Fig. 5 shows the graph of the solution region when $\alpha=20$ deg., $m_n=2.0, z_1=49, z_{2A}=50, k=0.3$. By picking out a point inside the region on the graph, the solution for $h_{kg1}+x_1$ and $h_{kg1}+h_{kg2A}$ satisfies the conditions. Additionally, the value of k can be small as far as the available solution exists on the graph.

As the next step, we consider the situation where the values of $\alpha, m_n, z_1, z_{2A}, k, h_{kg1}+x_1, h_{kg1}+h_{kg2A}$ are given. As mentioned above, when $k=x_{2A}-x_1$ is given, $x_{2B}-x_1$ is determined subordinately. If the values of h_{kg1} and h_{kg2B} are decided additionally to these values, the profile shift coefficients and addendum coefficients of all gears are determined. Here, we propose a graph with the horizontal axis h_{kg1} and the vertical axis h_{kg2B} in order to visually show the solution region at this step. The conditions that constrain these variables are Eqs. (19), (21)–(23), (25), and (27), and then the solution region is given by describing these inequalities on the proposed graph. Figure 6 shows the graph when $h_{kg1}+x_1=-0.84$ and $h_{kg1}+h_{kg2A}=0.96$ are selected from Fig. 5.

Once $x_1, x_{2A}, x_{2B}, h_{kg1}, h_{kg2A}, h_{kg2B}$ are determined by using Figs. 5 and 6, the values of the root circle diameters d_{f1}, d_{f2A}, d_{f2B} can be easily chosen, because Eqs. (29)–(31) give the conditions for these parameters explicitly.

From the above, the parameters of each gear satisfying all conditions clarified in Section 3 are determined, that is, the reducer is designed.

4.2 Strength analysis

In Section 4.1, the design method based on the geometrical conditions for the gears of the reducer is clarified. On the other hand, the strength of the gears is also an important indicator in the design. The gears used in the proposed motor especially tend to have special tooth shapes different from the shapes of regular gears, because of the conditions that the gear pairs with small and no differences in teeth number share the external gear. Therefore, the effect of the tooth shapes on the strength should be taken into consideration in the design. In this section, by examining the strength of the gears corresponding to the design solutions satisfying the geometrical conditions, the regions of the design solution that not only satisfy the geometrical conditions but also realize excellent strength are clarified.

[DOI: 10.1299/xxx.2014xxx000x]

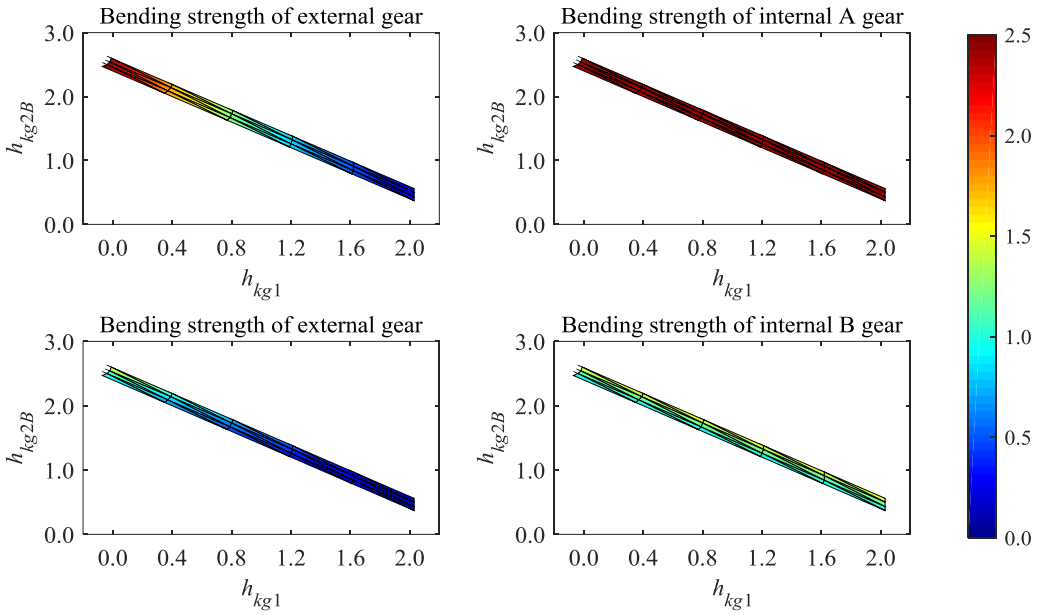

Fig. 7 Results of strength analysis on bending strength of the external gear and internal gears in Fig. 6. Upper graphs show the result of the engagement between the external gear and internal A gear. Lower graphs show the result of the engagement between the external gear and internal B gear.

A strength analysis is carried out with the K-H-V differential Gear Design System (AMTEC INC.). In this software, the tooth root bending stress σ_F is calculated based on the Japan Gear Manufacturers Association (JGMA) method (JGMA 401-01). The formula is as follows (The Japan Society of Mechanical Engineers ed., 1979):

$$\sigma_F = F_\mathrm{t} \frac{Y_F Y_\varepsilon Y_\beta}{m_n b} \left(\frac{K_V K_O}{K_L K_{FX}} \right) S_F \tag{32}$$

where F_t is the nominal circumferential force on the reference circle, Y_F is the tooth shape coefficient, Y_ε is the load distribution coefficient (the inverse of the contact ratio), Y_β is the helix angle coefficient, b is the facewidth, K_V is the dynamic load coefficient, K_O is the overload coefficient, K_L is the life coefficient, K_{FX} is the size coefficient to the tooth root stress, and S_F is the safety factor for tooth breakage. The analysis sets $Y_\beta = 1, K_V = 1, K_O = 1, K_L = 1, K_{FX} = 1, S_F = 1.2$. Other conditions are as follows: the torque applied to the external gear is $98\,\mathrm{N \cdot m}$, the revolution speed is $100\,\mathrm{min^{-1}}$, the facewidth of the external gear is $20\,\mathrm{mm}$, the facewidth of the internal A gear is $10\,\mathrm{mm}$, the total facewidth of the two internal B gears is $10\,\mathrm{mm}$, the root circle diameter of the external gear is the maximum value in Eq. (29), and the root circle diameters of the internal A and B gears are the minimum values in Eqs. (30), (31), respectively. The material of the gears is assumed to be induction-hardened S45C steel with 263 HV as the core hardness and 660 HV as the surface hardness. The allowable bending stress is $245\,\mathrm{MPa}$.

Not only the bending stress but also the contact stress, Hertzian stress, was calculated and taken into consideration (JGMA 402-01: The Japan Society of Mechanical Engineers ed., 1979). As a result of the analysis, however, the bending stress always reached its maximum allowable value before the Hertzian stress did. Therefore, we focus on the bending strength of the teeth, with the aim to construct the design method.

Figure 7 shows the result of the bending strength analysis for each gear corresponding to the solution region in Fig. 6. Figure 7 indicates the ratio of the allowable bending stress to the tooth root bending stress, which becomes higher when the strength is higher. Note that the bending strength is calculated on each node of the region in Fig. 7, and the graphs are filled by linear interpolation among the nodes. The upper graphs in Fig. 7 show the strength of the engagement of the external gear and the internal A gear. The strength of the external gear becomes higher when h_{kg1} becomes smaller. This could be because the arm length of the moment applied to the tooth root by the force on the tooth tip becomes short when the addendum is small, and then the bending stress becomes small. The strength of the internal A gear is constant over the entire region. The reason is that the bending stress on the internal A gear becomes constant under the condition in Fig. 6 that the values of $\alpha, m_n, z_1, z_{2A}, k, h_{kg1} + x_1, h_{kg1} + h_{kg2A}$ are determined. For the result of the engagement of the external gear and the internal B gear in the lower graphs in Fig. 7, the strength of the internal B gears becomes higher in the upper-right region. This distribution is similar to that of the contact ratio given

[DOI: 10.1299/xxx.2014xxx000x]

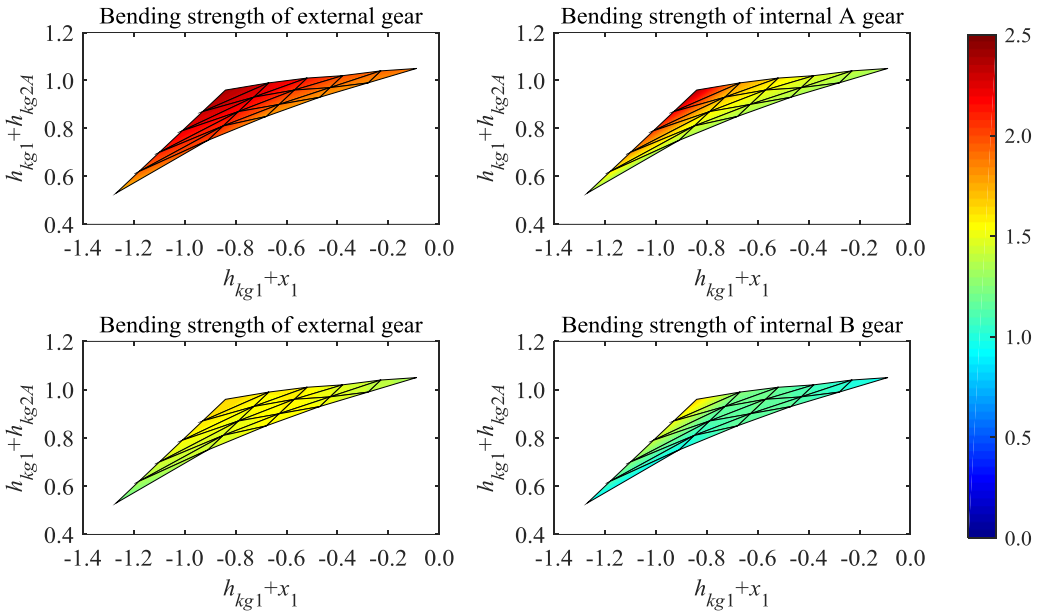

Fig. 8 Results of strength analysis on bending strength of the external gear and internal gears in Fig. 5. Upper graphs show the result of the engagement between the external gear and internal A gear. Lower graphs show the result of the engagement between the external gear and internal B gear.

by Eq. (25), possibly because the bending stress is distributed on some teeth of the internal B gears under the higher contact ratio. The strength of the external gear becomes higher in the upper region. The following two points are thought as the reason: the moment on the tooth root becomes small in the left region because the addendum gets smaller, as in the engagement with the internal A gear, and the loads are distributed in the upper-right region with the increase of the contact ratio, as in the internal B gears. The analyses with other conditions give results similar to those in Fig. 7. From the above, in the design using Fig. 6, we should choose a point from the upper-left of the solution region, especially from the point where h_{kg1} is small when the strength of the gear pairs including the internal A gear is prior, or from the point where h_{kg2B} is large when the strength of the gear pairs including the internal B gears is prior.

Next, the analysis result of the solution region in Fig. 5 is shown in Fig. 8. In the analysis, we assume that the point where h_{kg2B} becomes maximum is selected at the step of the design using Fig. 6. Figure 8 shows that the strength of the external gear, and the internal A and B gears becomes higher in the upper-left region. This distribution is the same as that of the contact ratio given by Eq. (24), and so the load distribution in the higher contact ratio could contribute to increasing the strength. Under other conditions, the results are similar. Therefore, in the design using Fig.5, we should pick out the point for the highest contact ratio in the upper left of the solution region satisfying the geometrical conditions.

In the way explained above, the best solution for the strength can be given in the design using Figs. 5 and 6.

4.3 Design algorithm

Based on the discussions in Sections 4.1 and 4.2, we next organize a design process for the gear pairs used in the proposed reducer-integrated motor. Figure 9 shows the flow chart of the entire design algorithm. First, the module m_n, the reference pressure angle α, and the teeth numbers z_1, z_{2A} are determined according to the requirements for the size of the motor or the reduction ratio. Then, we set the initial value of $k = x_{2A} - x_1$ as 0 and draw the graph for the conditions using $h_{kg1} + x_1$ and $h_{kg1} + h_{kg2A}$ as variables, as shown in Fig. 5. We check whether the solution satisfying the conditions exists in this graph. If no solution exists, we increase the value of k and redraw the graph. After obtaining the solution region satisfying the conditions, we choose the upper-left point as the solution for $h_{kg1} + x_1$ and $h_{kg1} + h_{kg2A}$. By using these values, we draw the graph for the conditions using h_{kg1} and h_{kg2B} as variables, as in Fig. 6. Similarly to the previous step, we again increase k and select parameters if the solution for the conditions is not given. After obtaining the solution region satisfying the conditions, we pick out a point from the upper-left region as the solution for h_{kg1} and h_{kg2B}. Up to this point, six parameters of $x_{2A} - x_1, x_{2B} - x_1, h_{kg1} +$

[DOI: 10.1299/xxx.2014xxx000x]

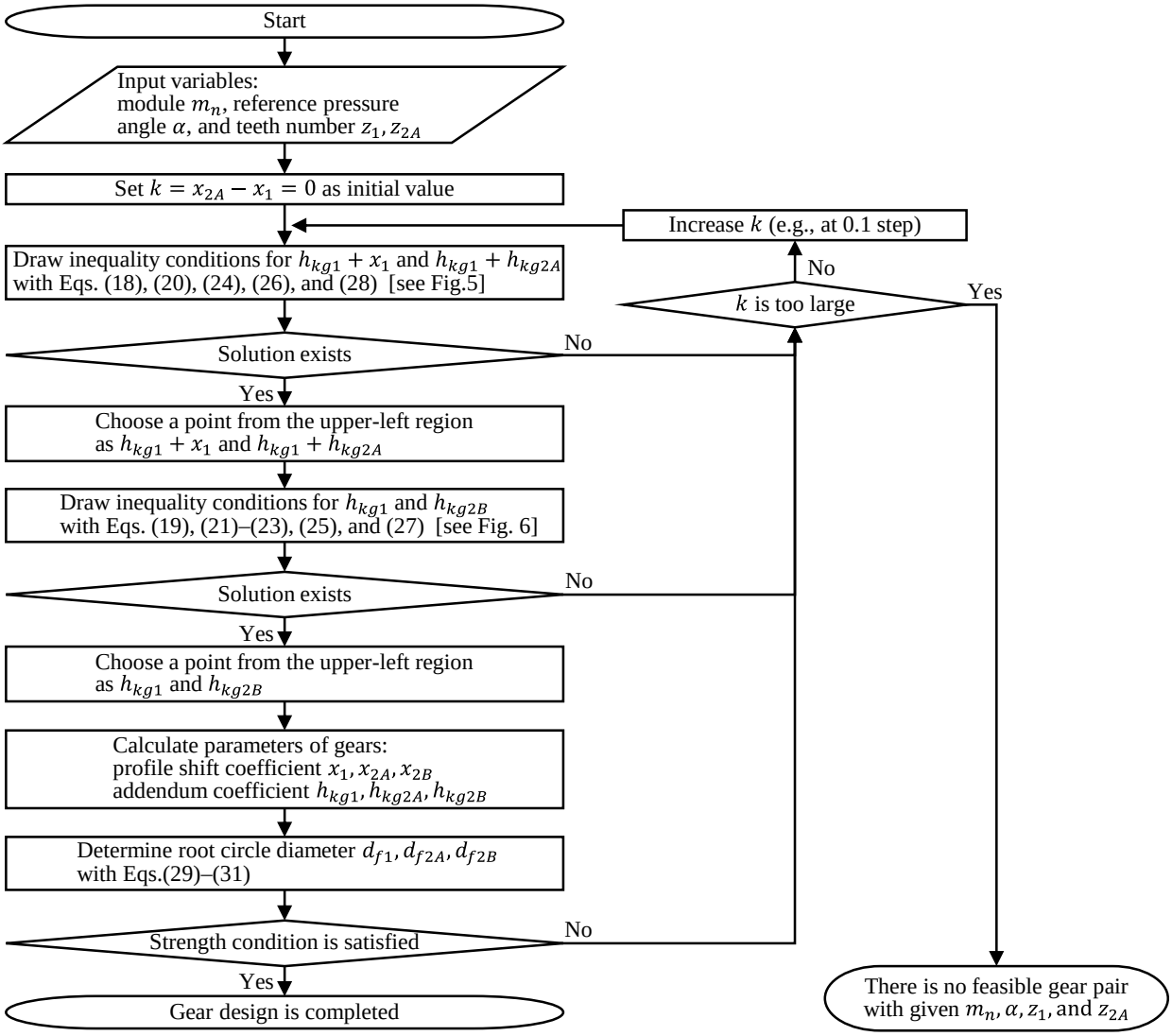

Fig. 9 Flow chart for designing the gears of the reducer used in the proposed reducer-integrated motor

$x_1, h_{kg1} + h_{kg2A}, h_{kg1}, h_{kg2B}$ are determined. By substituting each parameter, the profile shift coefficients x_1, x_{2A}, x_{2B} and the addendum coefficients $h_{kg1}, h_{kg2A}, h_{kg2B}$ are given. From Eqs. (29)–(31) assigning the given values, we determine the root circle diameters d_{f1}, d_{f2A}, d_{f2B}. Thus, the variables concerning the external gear, the internal A and B gears satisfying the all conditions are decided. Next, we carry out the strength analysis on each selected gear pair by providing the condition of use, such as the effective facewidth and load torque. Here, we check whether the tooth root bending stress is smaller than the allowable bending stress in each gear; if the strength condition is not satisfied, we again increase k and repeat the above steps. From the above process, the design of the gear pairs for the reducer of the proposed motor is completed. However, in the loop of calculations with increasing k, it is impossible to increase k unlimitedly. Therefore, if the conditions on the selection are not satisfied even with the maximum k, no feasible gear pair exists with the designated module m_n, reference pressure angle α, and teeth numbers z_1, z_{2A}. In this case, it is necessary to reconsider the requirements given first (e.g., to increase m_n).

5. Experiments and evaluation

5.1 Prototype

To verify that the proposed reducer-integrated motor works as expected, we conduct experiments using the prototype. The overview and properties of the developed prototype are shown in Fig. 10(a)–(d) and Table 1. In Fig. 10(d), the internal A gear is exposed by removing one of the two internal B gears and the external gear to show the internal structure. The basic structure of the prototype is the same as that in Fig. 2, and 12 linear actuators are installed.

[DOI: 10.1299/xxx.2014xxx000x]

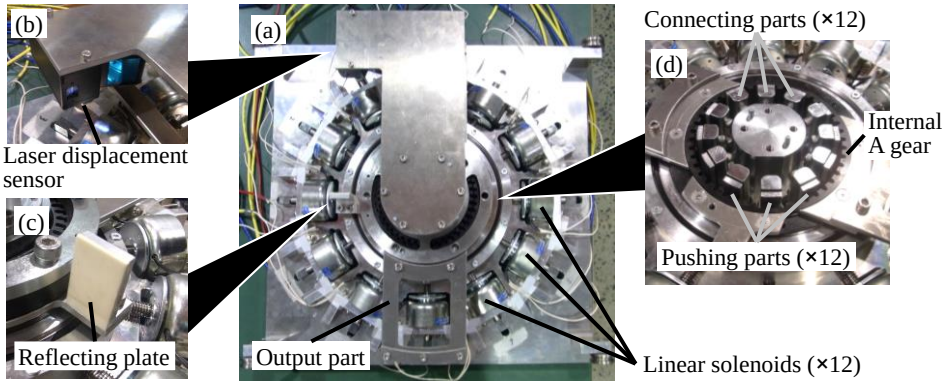

Fig. 10 Overview of the proposed reducer-integrated motor prototype

Table 1 Properties of the proposed reducer-integrated motor prototype

Entirety of prototype	Width	450 mm
	Depth	450 mm
	Height	150 mm
Linear solenoid	Model	Shindengen Mechatronics Co., Ltd., 6EF AWG. No. 20
	Input power	128 W
Laser displacement sensor	Model	KEYENCE Corporation, LK-G150
	Resolution	1 μm
	Sampling period	1 ms

Table 2 Specifications of the gears used in the proposed reducer-integrated motor prototype

	External gear	Internal A gear	Internal B gear
Module	3		
Reference pressure angle [deg.]	20		
Teeth number	43	44	43
Profile shift coefficient	-1.21	-0.91	0.7687
Addendum coefficient	0.60	0.35	2.0
Root circle diameter [mm]	115.14	132	132
Facewidth [mm]	52	26	12.5×2
Inner diameter [mm]	110.4	-	-
Outer diameter [mm]	-	170	170

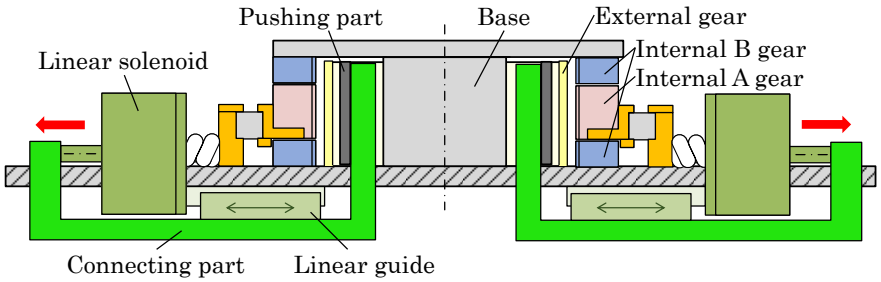

Fig. 11 Force transmission from linear solenoids to the external gear through linear guides, connecting parts, and pushing parts

Though we used linear solenoids as the linear actuators to gain large force output in order to confirm the movement in this prototype, the linear solenoids are put outside the gears because of their size. Hence, as shown in Fig. 11, the output of the linear solenoids is transmitted to the external gear through the connecting parts, which are supported by the linear guides to move in the radial direction, and the pushing parts, which have a semi-cylindrical shape and contact the external gear directly. The specifications of the produced gears are shown in Table 2. These gears are designed according to the method proposed in Section 4, and satisfy all the conditions clarified in Section 3. Figure 12 shows the tooth shapes of the gears calculated by the abovementioned software with the chosen parameters. The gears are made of NAK55 steel and processed by wire cut.

The operation of the prototype is controlled by a programmable logic controller (PLC). The prototype can switch the linear solenoids on and off instantly (i.e., less than 10 ms) by opening or closing the relays between the DC power source and the linear solenoids at the designated timing. Because it is connected to the laser displacement sensor, the PLC can measure the rotation angle of the output part. In the measurement of the rotation angle, the distance is measured between the laser displacement sensor fixed on the base (Fig. 10(b)) and the reflecting plate fixed on the

[DOI: 10.1299/xxx.2014xxx000x]

Fig. 12 Calculated result of the tooth shapes of the gears for the experiment. (a) External gear. (b) Internal A gear. (c) Internal B gear.

internal A gear and moving in the circumferential direction with the output part rotation (Fig. 10(c)). The displacement of the reflecting plate from the initial position in the progressing direction of the laser is converted into the rotation angle.

5.2 Experimental results and discussion

In the experiment, the linear solenoids are operated in the same way as in Fig. 3 and the internal A gear is rotated. The switching of the operating linear solenoids makes one cycle in the forward direction (clockwise) and one cycle in the reverse direction at 500-ms intervals per step. By substituting $n = 12, R = 44, T = 0.5$ s in Eq. (2), the theoretical value of the average rotational speed $\bar{N}$ is given as $\bar{N} \approx 3.8 \times 10^{-3}$ s^{-1}. According to visual observation of the movement of the output part, it was verified that the motor could rotate without any problem.

Figure 13 shows the measurement result of the rotation angle of the output part. In the figure, the blue line indicates the theoretical value and the red line indicates the measured value. Note that the results are offset so that the theoretical and measured values match at the initial time. The graph shows that the measured values nearly agree with the theoretical values for the entire time. This result verifies that the proposed reducer-integrated motor works as expected, and that the design method for the gears of the reducer proposed in Section 4 is effective fundamentally.

By taking a closer look at the graph in Fig. 13, small differences are seen between the theoretical and measured values. We discuss these differences by using the step angle errors. The step angle error is the difference between the theoretical and measured values in the step angle, that is, in the rotation angle of the internal A gear at each step. The theoretical step angle is $360/nR \approx 0.682$ deg. We repeated the same experiments shown in Fig. 13 ten times. Figure

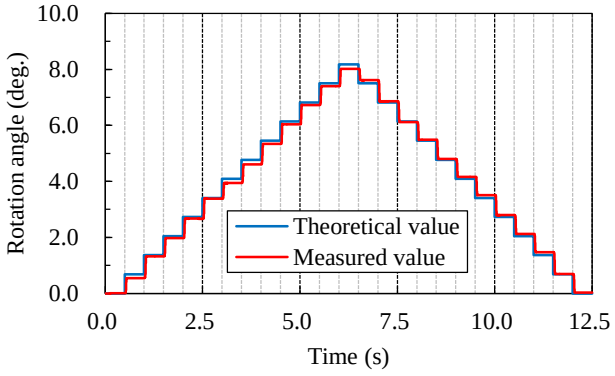

Fig. 13 Experimental result of output rotation angle over time

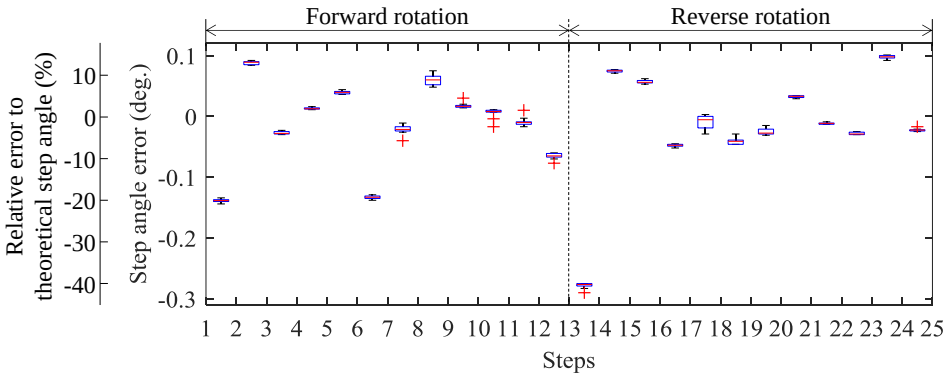

Fig. 14 Step angle errors in the experimental result

[DOI: 10.1299/xxx.2014xxx000x]

14 shows a box plot of the result of the collected step angle errors at each step. In this figure, the maximum length of the whiskers is restricted to 1.5 times the length of the boxes, and the data outside the regions are treated as the outliers, designated by + markers. The upper and lower fences show the maximum and minimum values of the data except the outliers. The horizontal axis indicates the step of switching the operating linear solenoids. As in Fig. 13, the former 12 steps are in the forward rotation, and the latter 12 steps are in the reverse rotation. The result shows that even though errors of outliers exist, the distributions of the errors in a certain step between the trials are smaller than the distributions of the errors in a certain trial between the steps. This means that almost the same errors occurred in ten trials of the experiments. This result suggests that the errors in the experiments are mainly caused by stationary factors, such as manufacturing errors or assembling errors. Additionally, in these experiments, the pair of two operating linear solenoids are the same at the i-th step in the forward rotation and the $(26-i)$-th step in the reverse rotation ($i = 1, 2, \cdots, 12$). However, the distribution of the step angle errors in Fig. 14 does not show the correlation between the errors in the forward and reverse rotations, and so the errors might be caused by gear shape errors or pitch errors of the manufactured gears. These errors could be suppressed by confirming the precision of the processed gears.

5.3 Evaluation of the load-supporting capacity

Based on the strength analysis procedure used in Section 4.2, the load-supporting capacity of the proposed motor is numerically evaluated in this section. The parameters of the analyzed gear pairs are the same as those of the produced gear pairs shown in Table 2, but their material is assumed to be induction-hardened S45C instead of NAK55 steel because we could not obtain sufficient data on NAK55 steel. The result of the analysis showed that the weakest point was in the engagement between the external gear and the internal B gear, and the maximum supportable torque is 457 N·m in terms of gear strength. In the proposed motor, the linear solenoids scarcely receive the circumferential force, so that the load-supporting capacity is thought to be determined by the strength of the gears. Therefore, the load-supporting capacity of the developed motor, i.e., the maximum supportable load torque applied to the output part, is calculated as $457 \times z_{2A}/z_1 \approx 467$ N·m.

If the linear solenoids need to support such load torque like the conventional reducer-integrated motors, the circumferential force applied to each linear solenoid is estimated to be $457/\left(12 \times d_{f1}/2000\right) \approx 662$ N. This is almost as large as the pushing force of the linear solenoids. Considering that linear solenoids are originally not designed to support lateral force, the estimated circumferential force should be beyond the capacity of the linear solenoids. In this way, the structure of the proposed motor leads to higher load-supporting capacity than that of the conventional reducer-integrated motors.

6. Conclusion

The motors for industrial robots need downsizing, large torque output, and high-precision positioning. However, conventional motors have difficulties in downsizing or supporting large torque. To solve these problems, we propose a novel reducer-integrated motor in this research. The proposed reducer-integrated motor uses a differential gear mechanism, in which two kinds of gear pairs with small and no differences in teeth number engage simultaneously. Linear actuators are installed inside the reducer. Two gear pairs with no difference in teeth number are fixed on the base and the gear pair with a small difference in teeth number is set between them. This structure of the motor contributes to downsizing of the entire motor system, high load-supporting capacity, and high stiffness. In this study, we conducted analyses and experiments on the proposed motor, and obtained the following results.

1) A novel reducer-integrated motor was proposed, and the structure and movement of the motor was explained.
2) The geometrical conditions for the gear pairs with small and no differences in teeth number sharing the external gear were clarified. The design method was proposed to acquire design solutions that satisfy the conditions from the graphs.
3) The strength of the gears corresponding to the design solutions was calculated and graphed. Solution regions realizing excellent strength were derived.
4) Based on the discussions on the geometrical conditions and the strength, a design algorithm for the gears of the reducer was constructed.

[DOI: 10.1299/xxx.2014xxx000x]

5) The experiments were conducted by using a prototype of the proposed reducer-integrated motor. The results verified that the prototype worked as expected, and that the proposed design method was effective fundamentally.

Acknowledgment

The authors would like to thank AMTEC INC. for their support in this research.

References

Barth, O., Harmonic piezodrive — miniaturized servo motor, Mechatronics, Vol.10 (2000), pp.545–554.

Doi, O., Ukai, T., Ochiai, H. and Kudo, H., Tooth profile interference and minimum teeth number of internal involute gear, Bulletin of the Faculty of Engineering, Hokkaido University, No. 81 (1976), pp.1–13 (in Japanese).

Hayashi, I., Iwatsuki, N., Kawai, M., Shibata, J. and Kitagawa, T., Development of a piezoelectric cycloid motor, Mechatronics, Vol.2, No.5 (1992), pp.433–444.

Ishida, M., Hori, T. and Hanaguchi, J., Principle and operation of the new type motor consisted of piezo-electric device and strain wave gearing, IEEJ Transactions on Industry Applications, Vol.110, No.12 (1990), pp.1247–1256 (in Japanese).

Kinki Gear Association ed., Design and Manufacturing of Gears (I) (1971), pp.23–24, TAIGA Publishing (in Japanese).

Morozumi, M. and Yaejima, K., Study on profile shifted involute internal gears having no difference in number of teeth between internal gear and pinion, Journal of the Faculty of Engineering, Shinshu University, No.27 (1969), pp.157–170 (in Japanese).

Morozumi, M., The theory and design calculation method of planetary gears and differential gears (1989), The Nikkan Kogyo Shimbun (in Japanese).

Ogino, S., A study on the involute spur gear of different center in equal speed, Transactions of the Japan Society of Mechanical Engineers, Vol.23, No.126 (1957), pp.88–93 (in Japanese).

Semba, M., Profile shifting of gears (1972), p.66, Kaihatusha Inc (in Japanese).

Suzumori, K. and Hori, K., Development of pneumatic wobble motors, JSME International Journal, Series C, Vol.42, No.2 (1999), pp.392–397.

Terakawa, T., Komori, M. and Morita, Y., Reducer-integrated motor using the principle of strain wave gearing system, Journal of Japan Society for Design Engineering, Vol.52, No.11 (2017), DOI: 10.14953/jjsde.2017.2737 (2017) (in Japanese).

The Japan Society of Mechanical Engineers ed., Technical Data Book: Design Data of Gear Strength (1979), pp.171–173 (in Japanese).

Yaejima, K. and Yano, A., Designing of generalized profile shifted involute internal gears, Journal of the Japan Society for Precision Engineering, Vol.57, No.1 (1991), pp.132–137 (in Japanese).

Yu, D., KHV planetary gear, Gear Technology, November/December 1987 (1987), pp.21–48.

Yu, D., KHV planetary gear - Part II, Gear Technology, January/February 1988 (1988), pp.28–48.

[DOI: 10.1299/xxx.2014xxx000x]